

Structural Analysis of the CC-130E Hercules During a Minimum Radius 60 Degree Bank Turn Flown by Major Michelle Colton

G03-FRCS-01

December 7, 2021

AE350: Analysis of Aircraft Structures

Group 03

Michael Akers (0917701)

Tyler Brooks (0759179)

Jack DiMeo (0866578)

Hunter Garramone (0874094)

Michael Madonia (0867010)

Clarkson University

8 Clarkson Ave

Potsdam, NY 13699

Abstract

The CC-130E Hercules is a Canadian variant of the Lockheed Martin C-130. The CC-130E entered service in the Royal Canadian Air Force (RCAF) in 1965, and was used primarily as a transport, navigation training, and search and rescue (SAR) aircraft [1]. The aircraft examined in this report currently resides at the National Air Force Museum of Canada and was flown by Major Michelle “Micky” Colton. Colton applied to be a pilot in 1980 only weeks after the RCAF began accepting female recruits [2]. Despite sexist criticism and pushback, Major Colton earned her pilot wings in 1982 and eventually accumulated over 7100 flight hours, 6936 of which were in the Hercules [3]. Major Colton typically flew as a SAR pilot while operating the CC-130E. Figure 1 shows Major Colton in the cockpit of the CC-130E.



Figure 1. Major Micky Colton Preparing to fly the CC-130E [4]

Considering aerodynamic, engine, and fuel loads, a clean, minimum radius 60 degree bank turn was determined to be the worst case loading scenario. This maneuver would have been performed by Major Colton as a SAR pilot or training officer [2]. The structural analysis of the starboard wing and horizontal stabilizer include beam bending, single-cell web-stringer, multi-cell web-stringer, and buckling models. Beam bending yielded no failure in the wing at normal maneuver airspeeds. With increased loading, failure in beam bending first occurred at slightly inboard of the engine closest to the fuselage of the aircraft. Web stringer analysis also yielded no failure at normal conditions. From web-stringer analysis failure first occurred in the leading edge spar of both the wing and stabilizer. Multi-cell and buckling analyses also indicated that no

failure would occur in the wing under normal loading. For both analyses, loading was increased to induce failure, showing that buckling would be the first failure mode of the wing. Buckling would first occur at a centripetal load of 1.92g. Locations of all failures are shown in Figure 2.

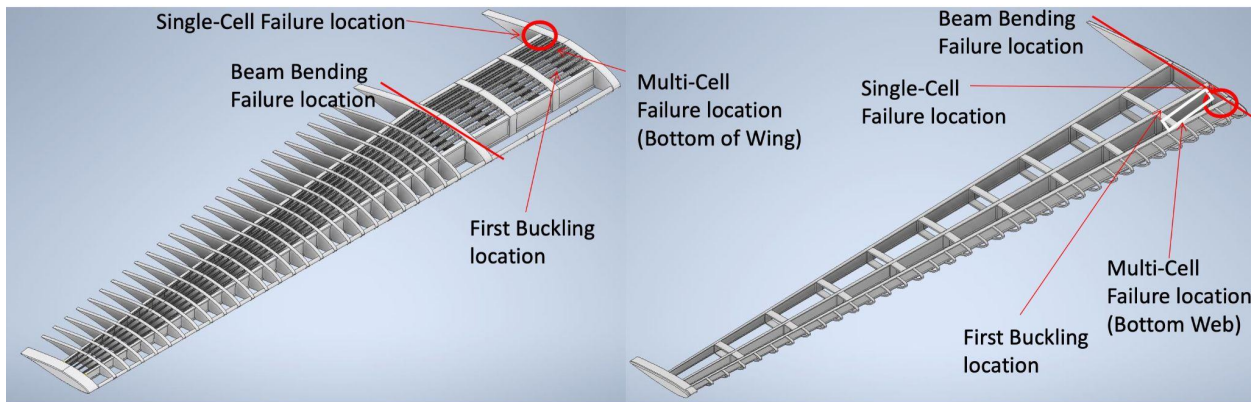


Figure 2. Wing (Left) and stabilizer (right) structure with failure locations highlighted

The same analyses were completed with respect to the starboard horizontal stabilizer. Similar to the results from the wing, no failure occurred under normal loading conditions during the minimum radius turn. Figure 2 shows the location of first failure from the beam bending, web-stringer, and column buckling analyses. The results that all analyses produced are not fully accurate. Many assumptions were made due to the lack of data found with respect to the exact dimensions and accurate aircraft data. These assumptions paired with those made to simplify the analyses result in potential inaccuracies in each of the calculations.

The group also considered the damaged conditions of each component in each analysis. In every case, the intact configuration required more loading to induce failure than the damaged arrangement.

Military aircraft, especially those built to perform in combat situations, are often designed to have extra structural redundancies to ensure flight in case of failures during combat. The C-130 platform is known for being a very robust and sturdy airframe with the ability to withstand many different scenarios. The results from the analyses are consistent with the nature of the aircraft, in that a loading increase from the maximum recommended centripetal acceleration was required to cause failures.

Table of Contents

1.0 Introduction.....	1
2.0 Major Micky Colton	1
3.0 Summary of the CC-130E.....	2
4.0 Applied Loads During Flight	4
4.1 Modeling Engine and Fuel Loads	4
4.2 Modeling Fuel Loads	5
4.3 Modeling Aerodynamic Loads	5
5.0 Beam Bending Analysis.....	6
5.1 Beam Bending Assumptions.....	6
5.2 Methods for Beam Bending	7
5.3 Results from Beam Bending Analysis	9
6.0 Single-Cell Web-Stringer Analysis.....	10
6.1 Single-Cell Web-Stringer Assumptions.....	10
6.2 Single-Cell Web-Stringer Methodology	12
6.3 Results for Single-Cell Web-Stringer Analyses	13
7.0 Multi-Cell Web-Stringer Analysis.....	15
8.0 Buckling Analysis.....	20
8.1 Sheet Buckling.....	21
8.1 Column Buckling Modeling and Methodology	21
8.2 Column Buckling Results	22
9.0 Conclusions from Analyses	23
List of References	25
Appendices.....	27

List of Figures

Figure 1. Major Micky Colton Preparing to fly the CC-130E [4]	i
Figure 2. Wing (Left) and stabilizer (right) structure with failure locations highlighted	ii
Figure 3. Major Colton in the cockpit of the CC-130E Hercules [3]	2
Figure 4. CC-130E Hercules at the National Air Force Museum of Canada [7]	3
Figure 5. Loads of the CC-130E wing (a, b) and stabilizer (c, d) during 60 degree bank turn	5
Figure 6. Starboard wing (left) and stabilizer (right) structure of the CC-130E Hercules	7
Figure 7. Effective stress in the starboard wing of the CC-130E	9
Figure 8. Effective Stress in starboard horizontal stabilizer	10
Figure 9. Single-cell simplification from real geometry of the starboard wing and horizontal stabilizer (a) to models from side (b) and rear (c) views	11
Figure 10. Single-cell Wing Stresses as a function of span under normal loading	14
Figure 11. Single-cell stabilizer stresses as a function of span under normal loading	14
Figure 12. Stress map of the web-stringer model for the wing root (a) and stabilizer root (b)	15
Figure 13. CC-130E structure (a) and multi-cell Model of the wing (b) and stabilizer (c) [15]	16
Figure 14. Multi-cell wing stringer stresses under normal loading conditions	18
Figure 15. Multi-cell wing web stresses under normal loading	19
Figure 16. Multi-cell stabilizer stringer stresses under normal loading	20
Figure 17. Multi-cell stabilizer web stresses under normal loading	20
Figure 18. Location of skin buckling on the starboard wing of the CC-130E [17]	21
Figure 19. Buckling locations in the starboard wing (left) and horizontal stabilizer (right)	22

List of Tables

Table 1: Magnitude of applied loads during maneuvers	6
--	---

1.0 Introduction

The CC-130E is a Canadian variant of the large cargo aircraft developed by the Lockheed Martin Corporation. In this report, the group outlines a brief history of the aircraft and a pilot of significance in the history of aviation, Major Michelle “Micky” Colton. Additionally, the stresses and failure of the aircraft's starboard wing and horizontal stabilizer during a 60-degree bank turn were analyzed. Analyses performed include beam bending, single-cell web-stringer, multi-cell web-stringer, and buckling models. The appendix contains a full set of engineering drawings.

2.0 Major Micky Colton

Maj. Micky Colton was born and raised in Kitchener, Ontario in 1958. Growing up, she initially had an interest in becoming a veterinarian. She first became interested in flying after she had the chance to cash in a free flying lesson from a book of coupons [2]. After having the chance to fly, she decided to leave her courier job for the Canadian Forces. Major Colton grew up in a decade of conservatism and post-war sexism [5]. Early on, when talking about her passion for military aviation, she was brought down by sexist criticism. As an example, Colton quoted her early life boyfriend “You can’t fly, you’re a girl” [2]. In addition to fighting the sexist criticism, major Colton is an indigenous woman, making her journey all the more difficult [6]. Nonetheless, Major Colton still pursued her passion to become a pilot. She applied to the Royal Canadian Air Force (RCAF) in 1980, only a few weeks after the Canadian Forces started accepting female civilian recruits to their pilot program [2].

Two years after applying to the RCAF, Maj. Colton received her pilot’s wings in 1982 and spent most of her time in the military as a SAR pilot, operating the CC-130 Hercules in Winnipeg, Edmonton and twice in Trenton [2][3]. Although the RCAF was accepting female pilots, there were still some who did not accept her. Major Colton mentioned, “There were officers then who didn’t want to see women get their wings and the air force “old boys’ club” was slow to embrace its newest members” [2]. Her service in the Air Force included time at 436 Squadron in Trenton, ON.; 429 Squadron Winnipeg, MB.; 435 Squadron Edmonton, AB.; 424 Squadron Trenton (twice); and 426 Squadron Trenton (twice) [2]. In 2000, Maj. Colton reached the 5,000-hour milestone with the C-130 and reached the 6,000-hour milestone in 2006 [5]. During her time in the Air Force, Maj. Colton said that harassment was common for the new female pilots such as herself, but by the time she retired women were treated as fellow

colleagues [2]. In an interview with the group, Major Colton pointed out that initially she was a “female pilot” but left the RCAF as a “pilot” [2]. After retiring from the regular force in 2011, Major Colton joined the Air Force Reserves one day later [3]. She then retired on May 30, 2018 as a Reservist Duty Operations Officer for 424 Transport and Rescue Squadron in Trenton [3]. She accumulated 6,936 hours on the C-130 Hercules before her retirement and, in total, logged more than 7,100 hours in the air [3]. Figure 3 shows Major Colton.



Figure 3. Major Colton in the cockpit of the CC-130E Hercules [3]

After retiring from the Air Force Reserves, Major Colton attended St. Lawrence College in Kingston in 2013, studying in the veterinary assistant certification program [2]. Major Colton is a mother and is married to Lieutenant Colonel Chris Colton, who she met through the Air Force as he was her first flight instructor back in 1982 [5]. Colton went on to become the owner of Horse Sense Equine business in Prince Edward County in Ontario and published a children’s book based on one of her horses called *Riley and the Road Cones* in 2021 [6].

3.0 Summary of the CC-130E

The Lockheed C-130 Hercules, designed in the early 1950s, is known as one of the most successful military transport aircraft ever designed [1]. The aircraft was used around the world, and has been shown to be extremely durable and reliable. After the aircraft’s success, the Royal Canadian Air Force ordered several C-130 Hercules in the 1960s [1]. Among these aircraft is the oldest Canadian variation of the C-130 Hercules, the CC-130E, which entered service in 1965

and served as a transport, navigation training, and SAR aircraft [1].

In the RCAF the CC-130E has held many roles. One aircraft flew with 435 Squadron in CFB Namao, Alberta, the 429 Squadron at CFB Winnipeg, and was used by the Air Navigation School. This aircraft was one of four Hercules that were modified to train navigators. In 1993, it was converted into a search and rescue airplane for 424 Squadron at CFB Trenton, Ontario [1]. This Hercules was the last of the CC-130Es and the oldest Hercules used by the RCAF, accumulating more than 47,000 hours of flight time in over 50 years of service [7]. A similar CC-130E, shown in Figure 4, is housed at the National Air Force Museum of Canada, in Trenton [1].



Figure 4. CC-130E Hercules at the National Air Force Museum of Canada [8]

The CC-130E Hercules offered to the National Air Force Museum of Canada was primarily used for heavy transport. The aircraft was originally owned by the USAF, but entered service with the RCAF in 1965 and served with various squadrons, including 435 squadron at CFB Edmonton, Alberta and then with 413 squadron in Greenwood, Nova Scotia. It flew for the last time in March 2010 and was then used in the Flyable Storage Program at CFB Trenton for loadmaster training and was fully retired in June 2010. It has been on display in the National Air Force Museum of Canada since 2011 [8].

The CC-130E is equipped with four, 24-stage axial Allison T56-A-7 turboprop engines and is able to fly up to speeds of 555 km/h [8][9]. Each wing consists of four fuel storage tanks allowing the C-130 to travel farther distances for longer periods of time whilst allowing it to carry payloads weighing up to 42,000 pounds [9]. Aside from being used for cargo transport, the aircraft has the ability to perform tasks such as SAR, surveillance, reconnaissance, aerial

refueling, and maritime patrol [9]. This aircraft is designed to take-off and land at short, austere, and contested runways with cargo and/or personnel. In addition to being a SAR pilot, Major Colton flew the Canadian variant of the C-130 as a training officer and check pilot. Typical maneuvers for Major Colton included basic take-off and landing under normal configurations with low weight, and standard clean configuration banks, climbs, and dives [2].

4.0 Applied Loads During Flight

Several loading conditions on the starboard wing and horizontal stabilizer of the CC-130E Hercules were explored before structural analysis. The maneuvers examined included cruise, climb, dive, and a clean 60 degree, port bank turn. Since the 60 degree turn is relevant to SAR missions and may have been performed by Major Colton it was chosen for evaluation. The subsections of section 4.0 discuss the loading from the fuel and the engines as well as aerodynamic loads during all of the aforementioned maneuvers. For the scope of this project, structural analyses are only performed on the worst case loading scenario, the minimum radius 60 degree bank turn.

4.1 Modeling Engine and Fuel Loads

First, the engines on the wing were considered. Engine rotational speed and power are constant during flight at 13,820 RPM and 3131 kW, respectively [10]. The 60 degree bank turn was evaluated at a typical SAR turn speed of 92.6 m/s [11]. With this information, engine torque (T) was calculated using Equation 1.

$$T = \frac{60}{2\pi} \cdot \frac{P}{RPM} = \frac{60 \cdot 3131 \cdot 10^3}{2\pi \cdot 13820} = 2.16 \text{ kN-m} \quad (1)$$

Where P is the power of the engine in kW and RPM is the rotational speed of the engine.

Additionally, engine thrust (F_{Thrust}) was calculated using Equation 2.

$$F_{Thrust} = \frac{P}{V} = \frac{3131 \cdot 10^3}{92.6} = 33.8 \text{ kN} \quad (2)$$

Where V is the airspeed of the CC-130E. An important note is that the value calculated in Equation 2 is the maximum available thrust of each engine. Actual thrust is controlled by feathering the propeller blades [10]. Engine weight under normal conditions was found to be 8.63 kN per engine [12]. Figure 3 shows the relative location of the engine loads.

4.2 Modeling Fuel Loads

The CC-130E has four wing based fuel tanks. With the volume and dimensions of each tank along with the standard properties of the recommended MIL-T-5624 the fuel load distribution was determined [11]. The external tank was considered first. This pylon mounted tank was taken as a point load for the purposes of this project. The external tank created a load of 40.5 kN. The load from the auxiliary tank, closest to the root of the wing is 13.3 kN/m acting over 1.98 m. The secondary tank, located between the engine nacelles, has a distributed load of 9.76 kN/m acting over 3.66 m. The primary tank, located toward the tip of the wing, has a distributed load of 4.48 kN/m acting over 8.71 m. Relative locations of the fuel loads are depicted in Figure 5.

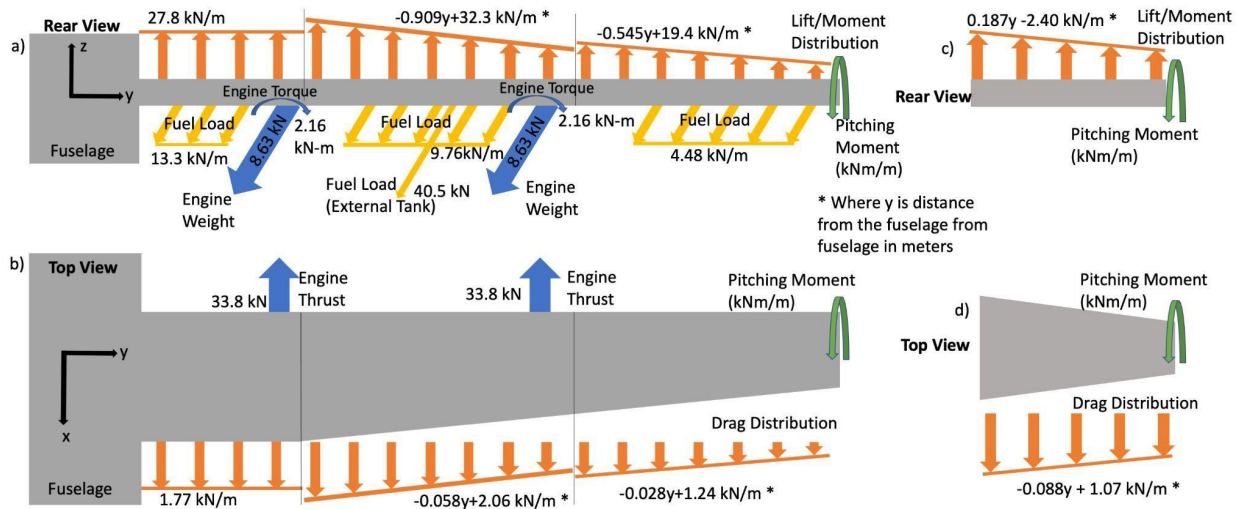


Figure 5. Loads of the CC-130E wing (a, b) and stabilizer (c, d) during 60 degree bank turn

4.3 Modeling Aerodynamic Loads

Each of the aerodynamic loads acting on the wing was calculated in three sections, accounting for the wing taper, geometric twist, and difference in airfoils from root to tip. Only one section was used to find the aerodynamic loads on the stabilizer. Lift was calculated using Equation 3, drag using Equation 4 and the pitching moment using Equation 5.

$$L = C_l \frac{\rho V^2}{2} A \quad (3)$$

$$D = C_d \frac{\rho V^2}{2} A \quad (4)$$

$$M = C_m \frac{\rho V^2}{2} A c \quad (5)$$

Where C_l , C_d , C_m , are the coefficients of lift, drag, and moment at the angle of attack for the maneuver, respectively. ρ is the density of the air, V is the airspeed, A is the planform area of the wing, and c is the chord length of the airfoil. The distributions of lift and drag during the clean 60 degree bank turn are shown in Figure 5. The moment is not shown, but shares similar distributions to lift. Integrating the distributed function yields the magnitude of the aerodynamic forces. Table 1 shows the resulting magnitudes for each maneuver. From these results the group determined the banking maneuver to be the worst case loading scenario.

Table 1: Magnitude of applied loads during maneuvers

Loads	Lift (kN)	Drag (kN)	Moment (kNm)
Wing - Cruise	308	34.4	96.3
Stabilizer - Cruise	10.4	8.33	2.47
Wing - Climb	364	31.9	126
Stabilizer - Climb	13.1	4.89	1.69
Wing - Dive	264	25.1	90.6
Stabilizer - Dive	9.52	4.11	0.242
Wing - Bank	395	25.2	101
Stabilizer - Bank	13.2	5.91	3.84

5.0 Beam Bending Analysis

Beam bending analysis was completed as the first solution to failure location along the span of the wing. While a failure along the span of the wing occurs, the component that fails is not determined by this analysis. Assumptions for this model are described in subsection 5.1. Subsections 5.2 and 5.3 outline the methodology of analysis and results for both the intact and damaged configurations, respectively.

5.1 Beam Bending Assumptions

To determine normal stresses from bending, the deflection in the z-direction was determined. Deflection was found using the Rayleigh-Ritz Method (R-R-M). The R-R-M is a

technique based on energy conservation principles and requires several geometric parameters. To use the R-R-M, several assumptions were made. Using the National Advisory Committee for Aeronautics (NACA) 64A318 and 64A412 airfoils for the root and tip of the wing, respectively, along with cutaway drawings of the structure a model of the wing was created in Autodesk Inventor. Figure 6 depicts a 3D rendering of the starboard wing and horizontal stabilizer structures which assumptions were based on.



Figure 6. Starboard wing (left) and stabilizer (right) structure of the CC-130E Hercules

Only using the spars, stringers, and skin, Autodesk Inventor was used to calculate the second moments of the area at several locations along the span of each component. A function was developed to describe the parameters at every point. The ribs were ignored for this model as they do not span the length of the wing. For this analysis the wing was considered as a cantilever, hollow beam made from 7075-T6 Aluminum [13].

5.2 Methods for Beam Bending

For both the intact and damaged configurations, R-R-M has four main steps. The first step is finding a kinematically admissible and continuous displacement field. To determine the displacement field, a continuous polynomial function with constant coefficients was used. Equation 6 shows the format for this function.

$$w(y) = a_0 + a_1y + a_2y^2 + \cdots + a_ny^n \quad (6)$$

Where $w(y)$ represents the displacement field, a_i is the i^{th} polynomial coefficient, and y is the location along the span of the wing. n terms are added to the assumed function. The cantilever beam model boundary conditions sets a_0 and a_1 equal to 0. The second step was to find the strain

energy in terms of the assumed displacement parameters. The function for strain energy with respect to displacement is shown in Equation 7.

$$U = \frac{EI}{2} \int_0^L \left(\frac{d^2w(y)}{dy^2} \right) dx \quad (7)$$

Where U is the strain energy, E is Young's Modulus of the material, I is the moment of inertia, and L is the span of the wing. The third step is to solve for the total potential energy (Π) in beam. Potential energy is found using Equation 8.

$$\Pi = U - W \quad (8)$$

Where W , work done on the beam, is found using Equation 9.

$$W = \int_0^L p w(y) dx \quad (9)$$

For work, the wing of the CC-130 is segmented in three segments. Each segment has a different load distribution in terms of span. Each section represents a different work function. The three functions are summed, resulting in equation 10.

$$W = \int_0^l p_1 w(y) dx + \int_{l_1}^{l_2} p_2 w(y) dx + \int_{l_2}^L p_3 w(y) dx \quad (10)$$

Where p_i is the distributed load applied across each section, and l_i is the lengths of the corresponding wing segment.

In the final step, the potential energy is minimized with respect to each polynomial coefficient using Equation 11.

$$\frac{d\Pi}{da_i} = 0, i = 1, 2, \dots, n \quad (11)$$

The displacement solution found with the R-R-M does not represent an exact solution; however, in minimizing the potential energy through multiple iterations of assumed displacement fields an approximate solution was found. A solution was considered to be accurate when the equation constants were within five percent of the equation constants from the previous iteration.

After convergence was found, the deflection field was used to calculate the stresses and strains in the modeled cantilever beam. Knowing the axial stresses allows for a maximum stress to be known and compared to Von Mises criterion for failure. Equation 12 shows the Von Mises failure criterion for the axial forces.

$$\sigma_{eff} = \sqrt{\sigma_{yy}^2 + 3\tau_{xy}^2 + 3\tau_{xz}^2} \geq S_y \quad (12)$$

Where S_y is the yield strength of the aluminum used for construction of the aircraft and σ_{eff} is the effective stress defined by axial stress, σ_{yy} , and shear stresses, τ_{xy} and τ_{xz} , acting on the

beam. Vertical deflection from lift contributed to σ_{yy} and τ_{xz} . Horizontal deflection contributed to σ_{yy} and τ_{xz} . The pitching moment contributed to τ_{xz} .

5.3 Results from Beam Bending Analysis

Figure 7 shows the effective stress plot of the wing modeled as a cantilever beam at standard flight conditions.

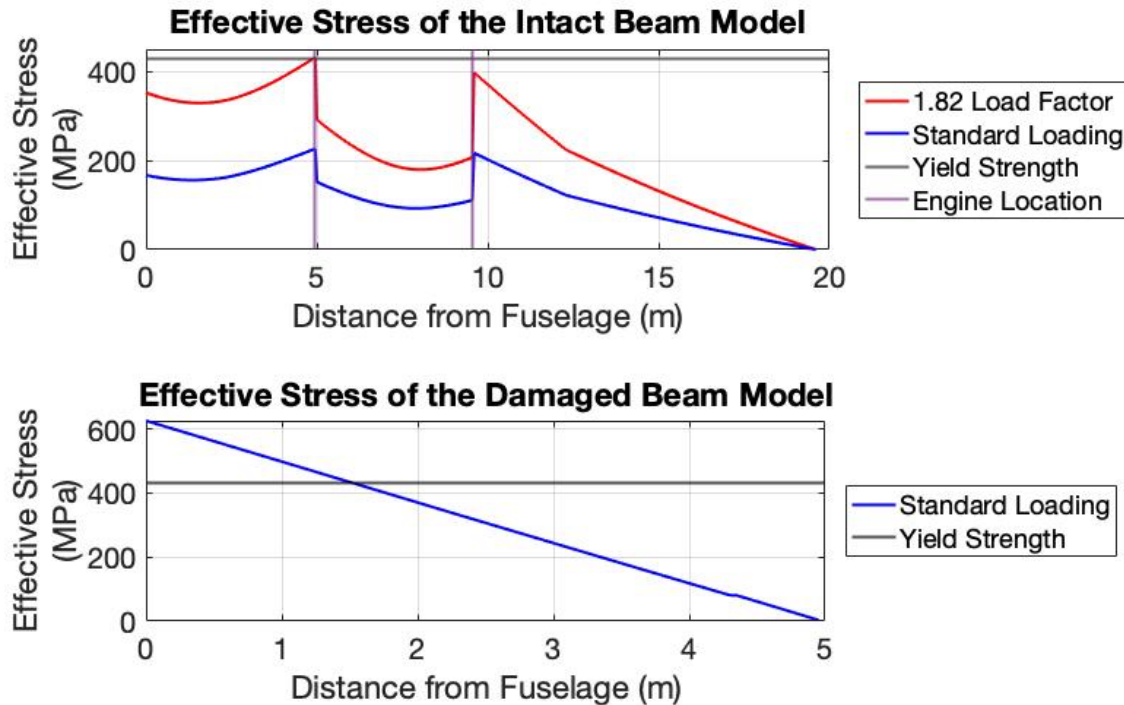


Figure 7. Effective stress in the starboard wing of the CC-130E

Using the Von Mises failure criterion the beam bending analysis indicates a location of first failure along the span of the wing. Failure is not expected to occur with the CC-130 banked at a 60° bank at standard speed of 92.6m/s. A maximum stress of 226 MPa occurred 4.95 m from the fuselage. To induce failure, the variable forces of lift, drag, and moment were increased by a factor of 1.82, corresponding to a 43.3 percent increase to the maximum allowable centripetal acceleration of 1.5g [12]. Damaged configuration results are dependent on the location of first failure of the intact configuration. Past the location of first failure the wing is no longer expected to hold the variable loads of lift, drag, and pitching moments. All variable loads were transferred to the undamaged portion of the wing for this analysis. Results indicate that stresses in the wing

reach 626 MPa at the root. These results indicate the structure would fail at standard flight conditions.

Figure 8 shows the effective stress plot of the horizontal stabilizer modeled as a hollow, cantilever beam. Under normal loading conditions there was no failure. An increase in the load factor of 6.16 was required to induce failure at the root of the horizontal stabilizer. As failure occurred at the root of the stabilizer a damaged condition could not be evaluated using the beam bending method.

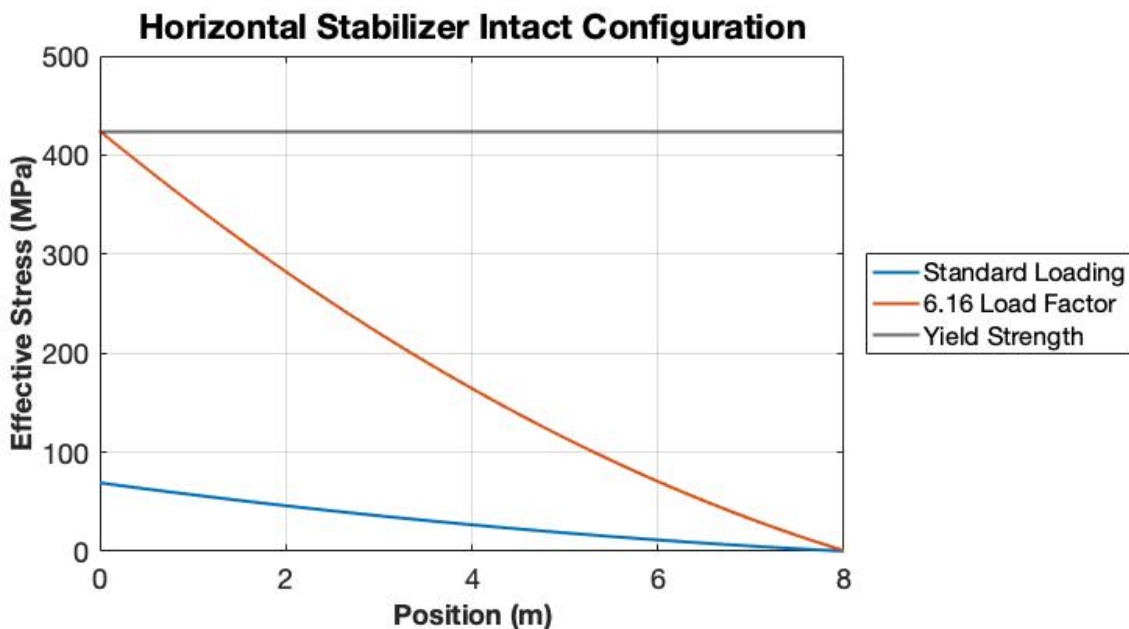


Figure 8. Effective Stress in starboard horizontal stabilizer

6.0 Single-Cell Web-Stringer Analysis

The web-stringer analysis completed in this report serves to provide a more accurate analysis compared to the beam bending model. For this report both the wing and horizontal stabilizer were modeled as simple box beams. Section 6.1 describes the assumptions made throughout the analysis, sections 6.2 and 6.3 report the methods and results for the analysis in both the intact and damaged configurations, respectively.

6.1 Single-Cell Web-Stringer Assumptions

The web stringer model calculated the stresses acting in the aircraft skin and stringers separately. For this initial calculation a simple box beam was modeled using spar and skin

dimensions. The spar flanges were connected by “webs” with thicknesses corresponding to the aircraft skin thickness on the top and bottom and spar thickness on the sides. Appropriate dimensions were found by working from cut-away representations of the CC-130E structure, as well as the Autodesk Inventor model shown in Figure 5. All components in this model were 7075-T6 Aluminum [14]. Figure 9 shows the single cell simplification of the horizontal stabilizer.

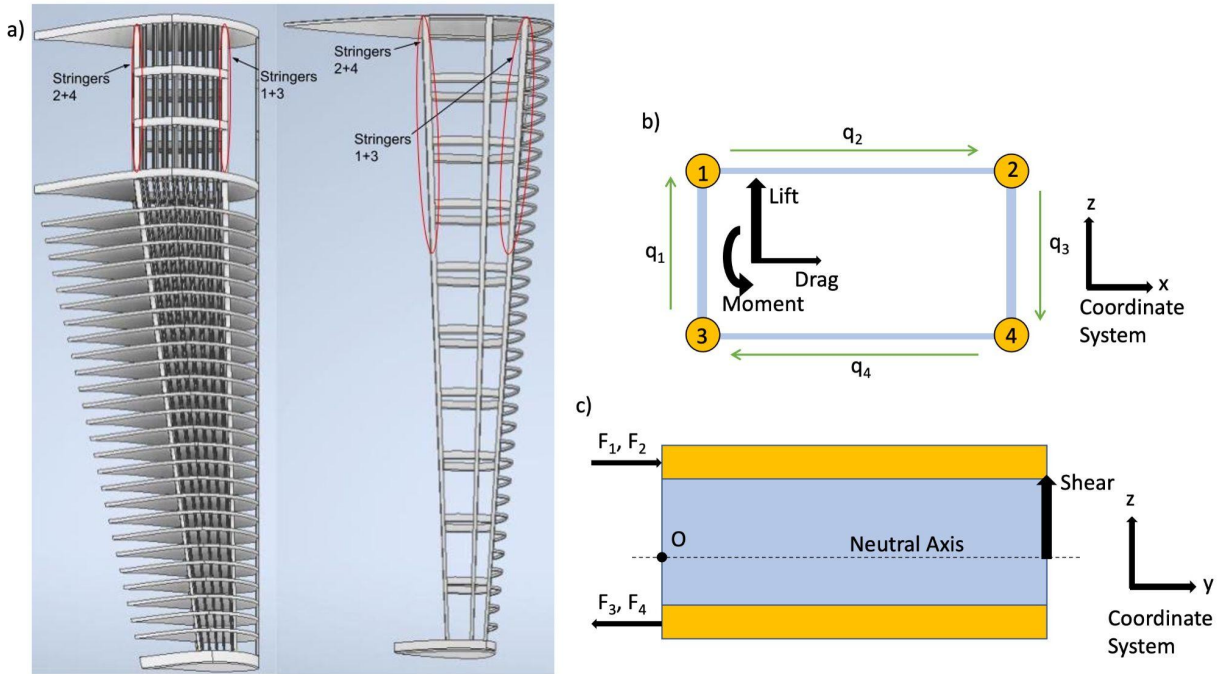


Figure 9. Single-cell simplification from real geometry of the starboard wing and horizontal stabilizer (a) to models from side (b) and rear (c) views

Figure 9.b shows the four modeled stringers of the single cell as well as the connecting webs. Additionally, shear forces and the moment are shown acting at the aerodynamic center. Figure 9.c shows the rear view of the unit length model with the neutral axis and shear force. The relative cross sectional shape for each component is depicted in Figure 12.

The major assumption made using web stringer analysis is that the stringers carry all of the axial forces whereas the modeled webs carry only the shear forces. The single-cell web-stringer model was performed at multiple stations along the span of each component.

6.2 Single-Cell Web-Stringer Methodology

After using the scaled cut-away isometric drawings to determine the cross sectional areas of the flanges in the model, Equation 13 was used to calculate the effective areas that compensate for the assumption that only the stringers carry axial forces.

$$A_{eff,i} = A_i + \Sigma \frac{b_j t_j}{6} \left(2 + \frac{\sigma_{i+1}}{\sigma_i} \right) \quad (13)$$

In Equation 13, A_i is the actual area of the cylindrical stringer i . b_j and t_j are the length and thickness of the webs neighboring stringer i , respectively. σ_i and σ_{i+1} are the stresses in stringer i and stringer $i+1$. Since stresses are not yet known the ratio is replaced by the ratio of distances of each stringer to the neutral axis. The location of the neutral axis was calculated with Equation 14.

$$\bar{Z} = \frac{\Sigma A_i z_i}{\Sigma A_i} \quad (14)$$

Where A_i is the cross sectional area of stringer i and z_i is the distance of stringer i from a reference axis.

Equation 15 describes an important relation between the forces in each stringer.

$$\frac{F_1}{A_1 d_1} = \frac{F_k}{A_k d_k}, k = 2,3,4 \quad (15)$$

In Equation 15, F represents the force in the respective stringer, A is the effective area of the stringer, and d is the distance between the stringer and the neutral axis.

A static moment balance about an axis through point O in Figure 9.c was taken. Equation 16 shows the form of the moment balance.

$$\Sigma M = 0 = \Sigma F_i d_i + F_{Shear} + M_{external} \quad (16)$$

Here, F_i and d_i are the unit length forces and moment arm for each stringer, i . F_{Shear} is the net shear force between the analysis point and the wing tip. $M_{external}$, in this case, is the external moment from engine torque. Solving using Equations 15 and 16 for F_1 yields Equation 17.

$$F_1 = \frac{-(F_{Shear} + M_{external})}{d_1 + \left(\frac{1}{A_1 d_1} \right) (\Sigma A_l d_l^2)}, l = 2,3,4 \quad (17)$$

Using the result from Equation 17 in Equation 15 allows for the calculation of all axial forces per unit length. The processes represented by Equations 14 through 17 were repeated in the X direction to account for axial forces caused by drag. Using superposition principles the unit length forces were then summed for each stringer. Multiplying the unit length forces by the length of the wing yielded total force in each stringer from shear forces. The 60 degree bank leads to a component of engine and fuel weights acting as a compressive force. The compressive

weight force was distributed evenly among the stringers. Axial stress was determined by dividing the axial force by the corresponding effective area. Equation 18 shows the Von Mises failure criterion for the axial forces.

$$\sigma_{yy} \geq S_y \quad (18)$$

Where S_y is the yield strength of the aluminum used for construction of the aircraft.

Shear flows in each of the webs was determined to find shear stress. Using free body diagrams, Equation 19 relating each of the shear flows to a reference shear flow (q_0) and known axial forces was developed.

$$q_i = q_0 + \Sigma F_i \quad (19)$$

A moment balance accounting for the shear flows, pitching moment, lift force, drag, and external forces was completed to determine the value of the reference shear flow. Using the relationship shown in Equation 19 the remaining shear flows were calculated. Shear stress in each web was calculated with Equation 20. Equation 21 shows the Von Mises failure criterion for a shear stress in the web.

$$\tau = \frac{q_i}{t_i} \quad (20)$$

$$\sqrt{3}\tau \geq S_y \quad (21)$$

6.3 Results for Single-Cell Web-Stringer Analyses

For the intact configurations a full box beam configuration with four stringers was used to model both the wing and horizontal stabilizer. Figure 10 shows the stress distribution of the wing as a function of span, accounting for taper and loading changes under normal conditions. The loading changes are represented by the vertical lines in the subplots of Figure 10.

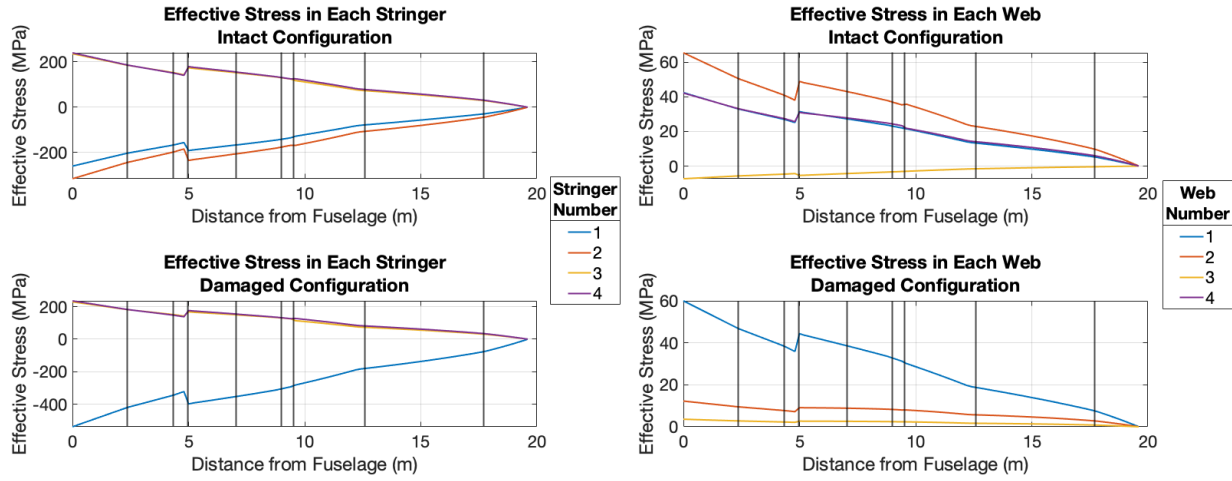


Figure 10. Single-cell Wing Stresses as a function of span under normal loading

Figure 11 shows the stress in the horizontal stabilizer as a function of the components span under normal loading from the clean, 60 degree bank turn.

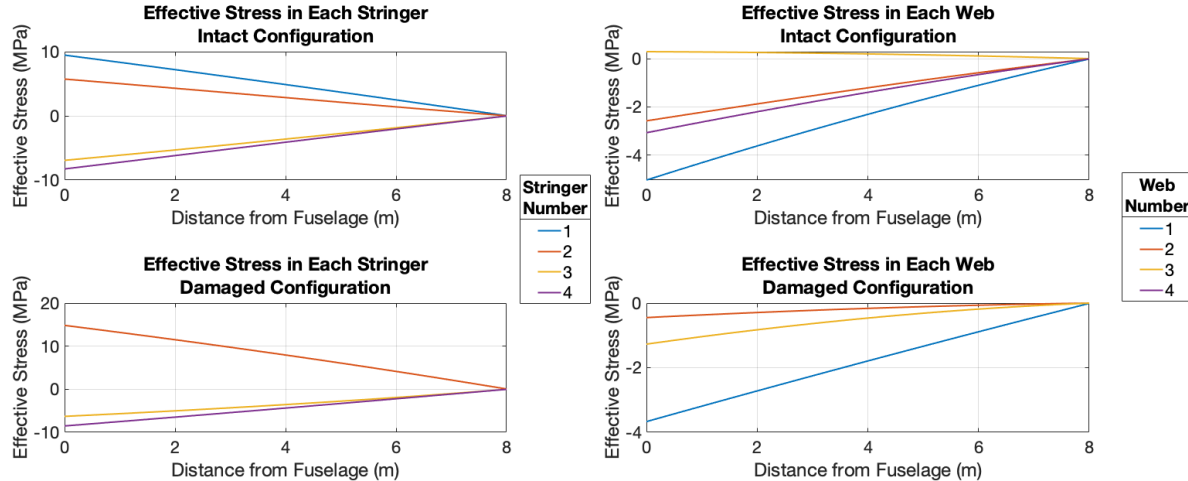


Figure 11. Single-cell stabilizer stresses as a function of span under normal loading

Figures 10 and 11 show that in both the starboard wing and horizontal stabilizer the highest stresses occur at the root. Stress maps of the single-cell web-stringer model for both components in their intact and damaged states are shown in Figure 12.

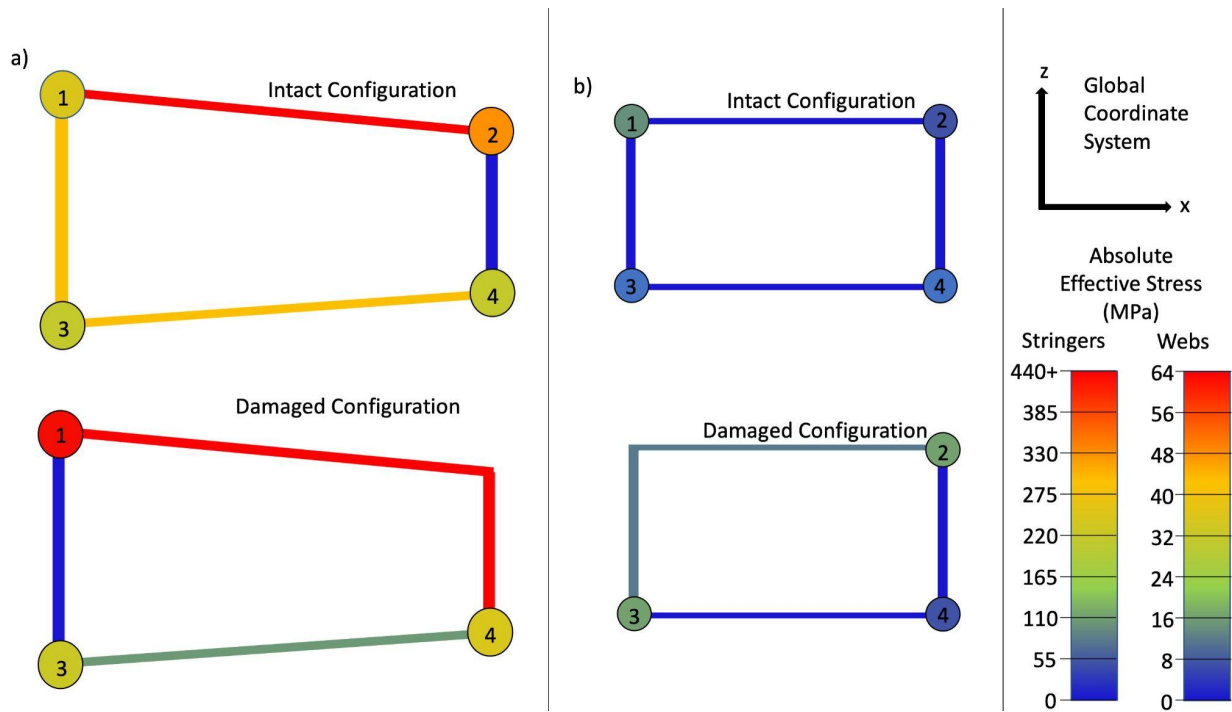


Figure 12. Stress map of the web-stringer model for the wing root (a) and stabilizer root (b)

In the starboard wing, failure was not found during the clean 60 degree bank turn at a standard speed of 92.6 m/s. Failure first occurred in the top stringer towards the leading edge of the wing at an airspeed of 104 m/s while maintaining a turn radius of 583 m. At this point, stress exceeded the 430 MPa yield strength of the aluminum. The speed at failure corresponds with a 28.4 percent increase from maximum recommended centripetal acceleration [11]. By removing the failed stringer at the root, a damaged configuration of the wing was analyzed. Failure of the wing root does occur in the normal loading condition in the damaged state. The second instance of failure occurs at the root in the top stringer toward the trailing edge.

The starboard horizontal stabilizer was analyzed for failure separately from the wing. Under normal conditions, no failure was detected in the stabilizer root. While maintaining the 583 m turn radius failure occurred in the top, leading edge stringer at an airspeed of 227 m/s. After removing the failed stringer, the stabilizer was analyzed again in a damaged state. In the damaged state the root of the stabilizer failed at an airspeed of 191 m/s.

7.0 Multi-Cell Web-Stringer Analysis

The subsections of Section 7 describe the multi-cell web-stringer analysis in its entirety. Subsection 7.1 describes the necessary assumptions, models, and methodology. Subsection 7.2

reports the results of the analysis on the starboard wing and stabilizer.

7.1 Modeling and Methodology

Multi-cell web-stringer analysis allowed stress in the stringers, spars, and skin of components to be analyzed. Simplified models of the wing and stabilizer at their roots for the intact condition are shown in Figure 13.

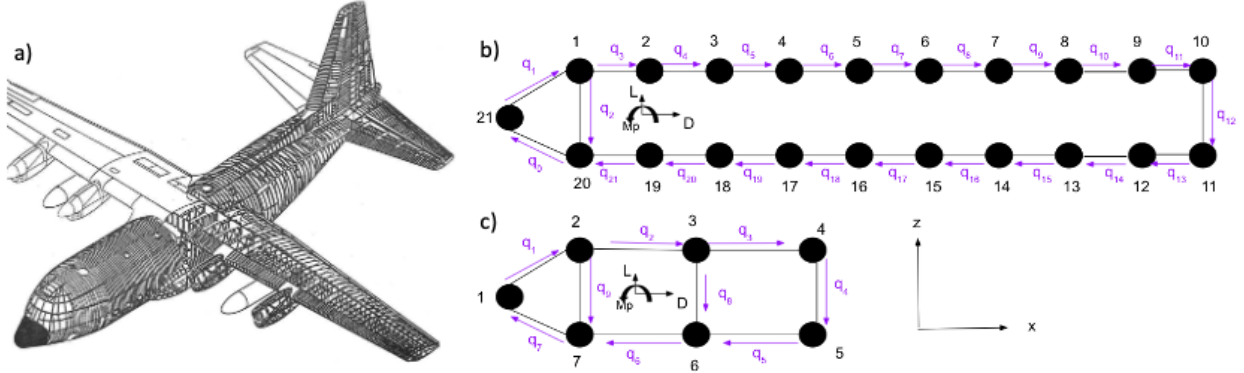


Figure 13. CC-130E structure (a) and multi-cell Model of the wing (b) and stabilizer (c) [15]

In Figure 13.b and 13.c each dot represents a stringer or spar flange, and the connecting “webs” represent the skin or spar. Geometric parameters were derived from isometric views of the C-130E as shown in Figure 13.a. The thickness of each web corresponds to skin thickness for the perimeter and spar thickness for the interior webs. The shear forces and moments are shown acting through the aerodynamic center of each component. All materials in this model were assumed to be 7075-T6 Aluminum [14].

First, an effective area of each stringer was calculated using Equation 22.

$$A_{eff,i} = A_i + \sum \frac{b_j t_j}{6} \left(2 + \frac{\sigma_{i+1}}{\sigma_i} \right) \quad (22)$$

Where A_i is the cross sectional flange area of the i -th stringer. b_j and t_j are the length and thickness of the webs neighboring the i -th stringer, respectively. σ_i and σ_{i+1} are the stresses in the i -th stringer and the next stringer, $i+1$. Since stresses are not yet known the ratio is replaced by the ratio of distances of each stringer to the neutral axis.

Equation 23 describes the relation between the forces in each stringer.

$$\frac{F_1}{A_1 d_1} = \frac{F_k}{A_k d_k}, k = 2, 3, 4, \dots, n \quad (23)$$

In Equation 23, F represents the force in the respective stringer, A is the effective area of the stringer, d is the distance between the stringer and the neutral axis, and n is the number of stringers in the model

A static moment balance about the point where the neutral axis meets the reaction plane was taken. The general form is shown in Equation 24.

$$\Sigma M = 0 = \Sigma F_i d_i + F_{Shear} + M_{External} \quad (24)$$

Here, F_i and d_i are the unit length forces and moment arm for each stringer, i . F_{Shear} is the net shear force between the analysis point and the wing tip. $M_{External}$, is any external moment. Solving Equations 23 and 24 yields force per unit length in each stringer. Multiplying by the distance from the analysis point to the wing tip gave total forces. Dividing each force by the respective area of each stringer resulted in the axial stress at the analysis location.

Using the models shown in Figure 13, a reference shear flow was selected in each cell and relations were developed using static force analysis. Compatibility was used to equate the angle of twist in each cell. The angle of twist is calculated with Equation 25.

$$\theta = \phi \frac{q_i}{2AGt_i} \quad (25)$$

Where q_i is the shear flow in web i , A is the area enclosed by the cell, G is the shear modulus of the material, and t_i is the thickness of web i . Applying a torque balance as shown in Equation 26 with compatibility and the shear flow relations, shear flow was found.

$$T = \Sigma 2A_i q_i \quad (26)$$

Where A_i is the area enclosed by an arbitrary torque location, and the two stringers connected by the web being evaluated. Dividing shear flows by respective web thicknesses yielded effective stress. Von Mises failure criterion was then used to determine failure for webs and stringers.

7.2 Multi-Cell Results

For the wing the stresses were evaluated at locations of geometry change or abrupt loading changes, such as an engine or fuel tank, as well as several other locations along the wing. The highest stress of 212 MPa was found in stringer 16 at the root. Failure occurred in stringer 16 when variable loads were multiplied by a factor of 1.96. The highest web stress was found to be 107 MPa. Removing stringer 16 from the model simulated the damaged state of the wing. For

the damaged state, failure did not occur under normal conditions, but only required a loading factor of 1.64 to induce failure in stringer 15. Figures 14 and 15 show the interpolated stresses in each stringer and web of the wing as a function of span, locations of loading or geometry changes are represented by the vertical lines in each of the subplots.

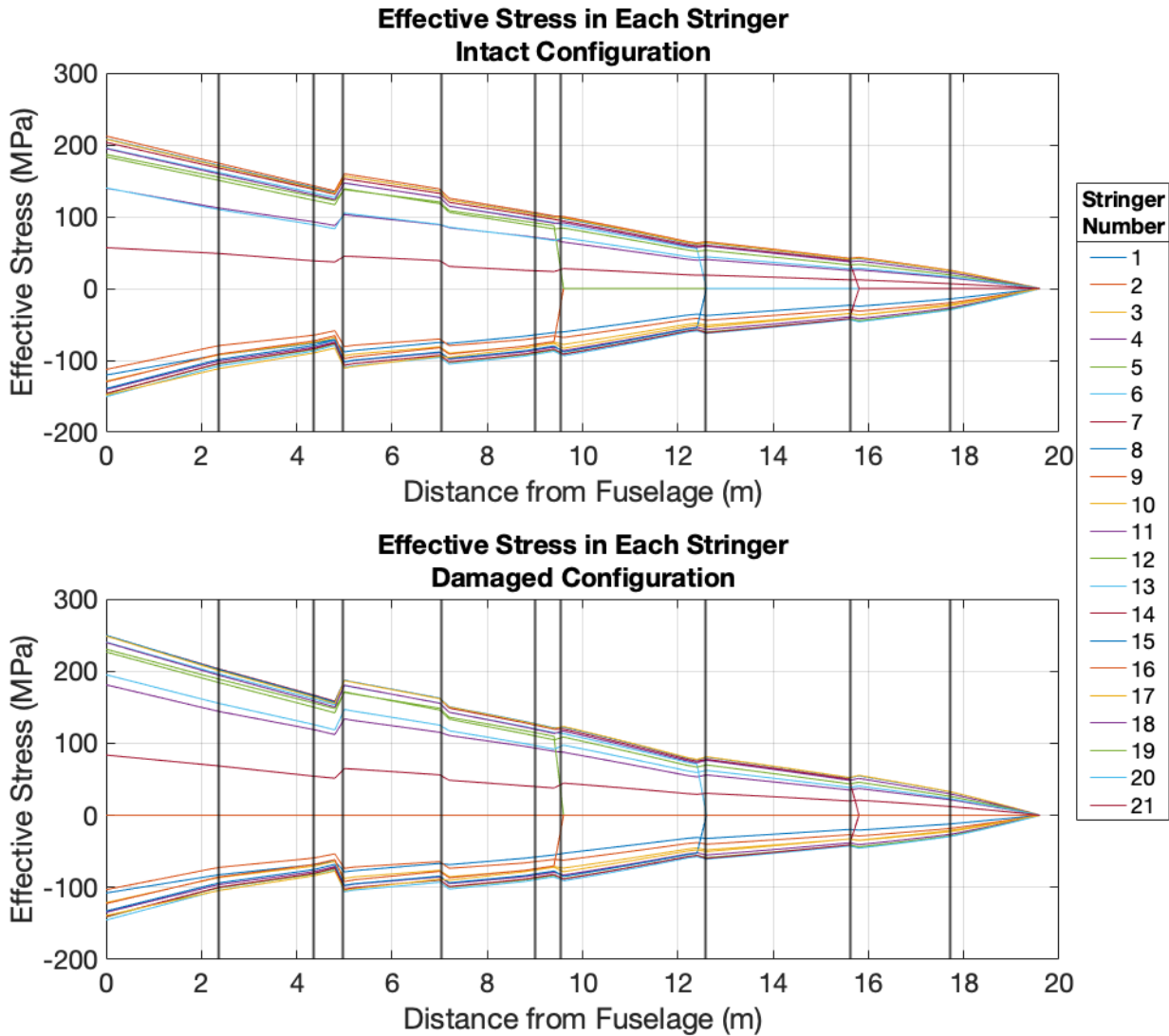


Figure 14. Multi-cell wing stringer stresses under normal loading conditions

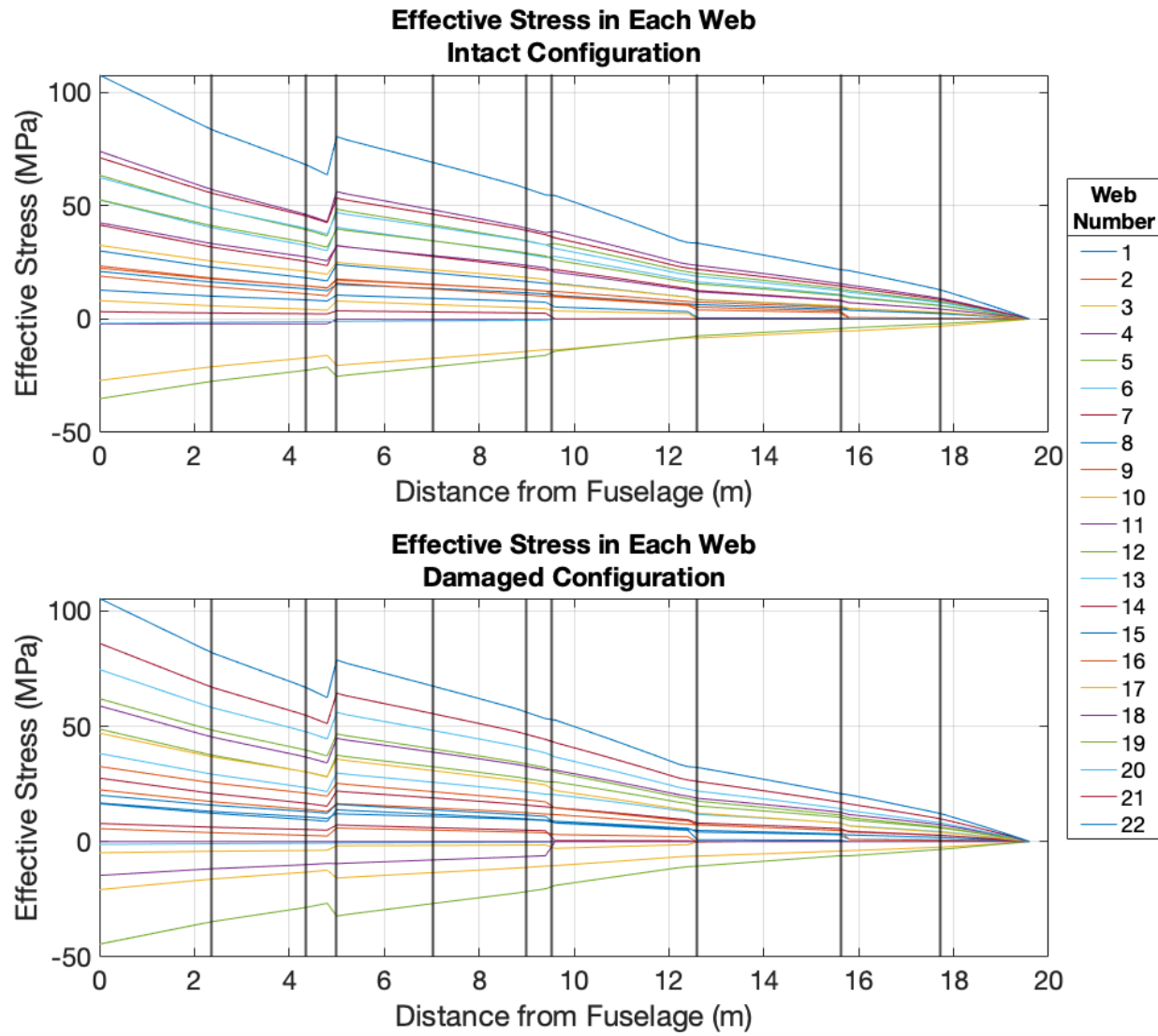


Figure 15. Multi-cell wing web stresses under normal loading

The horizontal stabilizer was evaluated at eight locations along its length, each one meter apart. The first analysis point was at the fuselage. At normal loading conditions, the highest stress was found to be 46.7 MPa in web 6 at the stabilizer root. Web 6, shown with q_6 in Figure 13.c, reaches its yield strength of 430 MPa at the root when the applied loads are multiplied by 5.85. At the normal loading conditions, the highest axial stress is 1.06 MPa in stringer 6. Web 6 was removed from the geometry to create a damaged condition. At normal loading, web 2 failed with a maximum shear stress of 840 MPa in web 2. The highest axial stress was 29.6 MPa in stringer 6. Figures 16 and 17 show the stresses in the elements present in the rear stabilizer along its span.

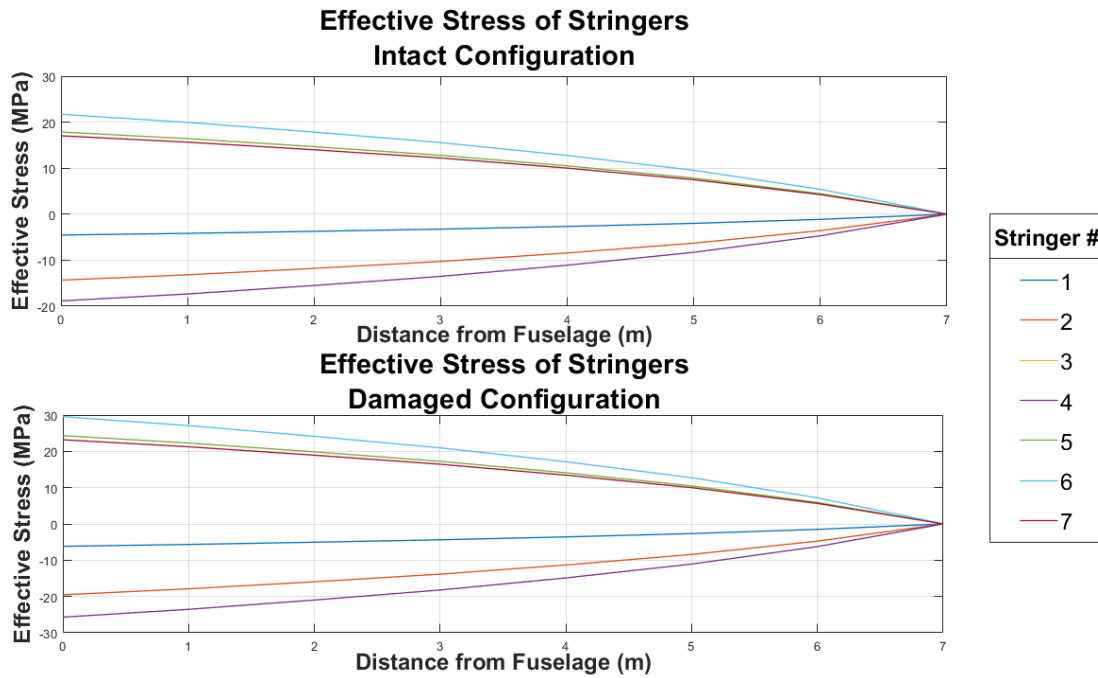


Figure 16. Multi-cell stabilizer stringer stresses under normal loading

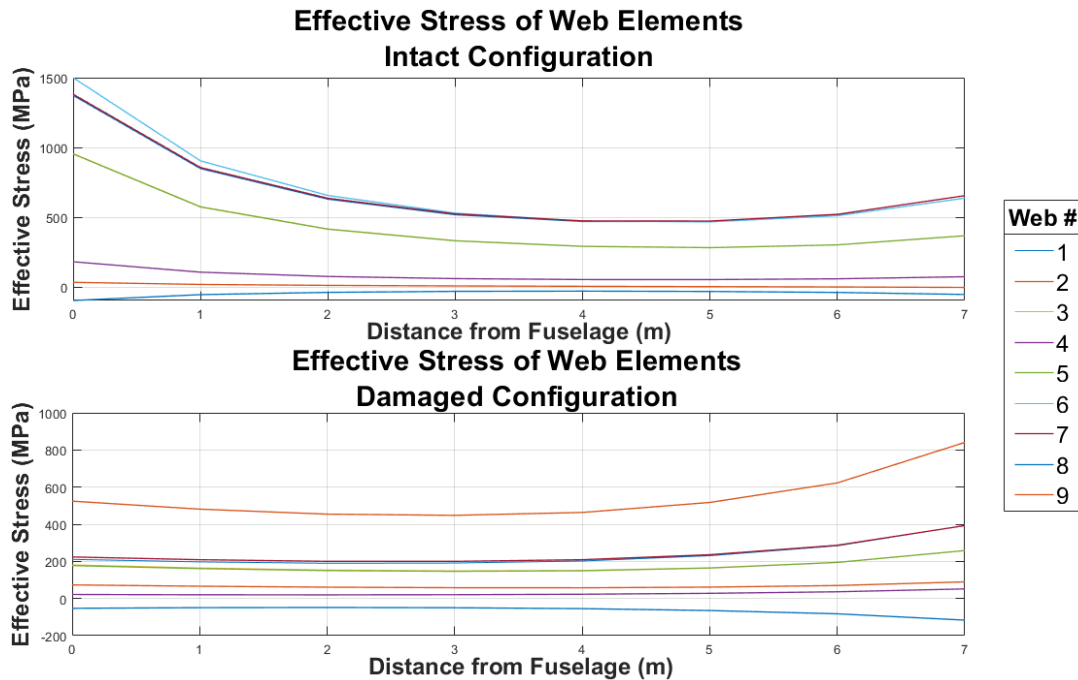


Figure 17. Multi-cell stabilizer web stresses under normal loading

8.0 Buckling Analysis

Subsections 8.1 and 8.2 describe the buckling analysis. Subsection 8.1 describes the

modeling and methodology of the process. Subsection 8.2 presents the results of the analysis for the starboard wing and horizontal stabilizer in their intact and damaged conditions.

8.1 Sheet Buckling

To evaluate the sheet buckling of the starboard wing and horizontal stabilizer the shear stresses found in each of the webs with the multi-cell web-stringer analysis were considered. Critical buckling loads were found by comparing the given shear stresses to critical buckling loads published by Boeing [16]. On the wing, sheet buckling occurs in the leading edge panel inboard of the first engine, the location is shown in Figure 16. No other panels experience buckling under normal loading conditions. On the stabilizer, sheet buckling does not occur under normal loading conditions.



Figure 18. Location of skin buckling on the starboard wing of the CC-130E [17]

8.1 Column Buckling Modeling and Methodology

All components were considered to be 7075-T6 Aluminum [14]. To calculate the critical buckling loads the Euler, Rankine-Gordon, Straight-line, and Johnson methods were considered. To determine the most accurate critical load calculation method the slenderness ratio was calculated with Equation 27.

$$R = \frac{L}{k} \quad (27)$$

Where R is the slenderness ratio, L is the distance between the end conditions, k is the radius of gyration of the cross section. For stringers, end conditions were assumed to be pinned at each rib. For spars, end conditions were assumed to be fixed at the fuselage and free at the component tip.

Given the calculated slenderness ratios of the components, the Johnson Parabola was considered the most accurate estimation of buckling in the stringers ($R < 48$), the form of the Johnson parabolic curve is described by Equation 28.

$$P_{cr} = \sigma_a A \left(1 - \frac{\sigma_a}{4\pi^2 EI} \left(\frac{L}{k} \right)^2 \right) \quad (28)$$

Where P_{cr} is the critical buckling load of the member, σ_a is the yield strength, E is the modulus of elasticity, A is the cross sectional area, and C is the restraint coefficient. For the pinned-pinned end conditions of the stringers, $C=1$ [18]. Euler's Method was used to determine critical buckling loads in the spars ($R > 48$). Euler's Equation is shown in Equation 29.

$$P_{cr} = \frac{n^2 \pi^2 EI}{4L^2} \quad (29)$$

Where n is the number of supports ($n=1$ for spars) and I is the second moment of the area. Once critical loads were determined with the appropriate method, the critical loads were compared to the forces obtained during the multi-cell web-stringer analysis.

8.2 Column Buckling Results

In the intact state of both the starboard wing and horizontal stabilizer neither component would buckle under normal loading conditions. For the intact states of the wing and stabilizer, the variable loads were increased by a factor of 1.56 and 17.5 to induce buckling in each component, respectively. The damaged conditions found in the multi-cell web-stringer analysis were used as the damaged condition for buckling calculations. Buckling of the damaged states occurred in the wing when variable loads were increased by a factor of 1.48 and in the stabilizer under the normal loading conditions. Figure 17 shows the location and loading factor required to induce buckling with each calculation method.

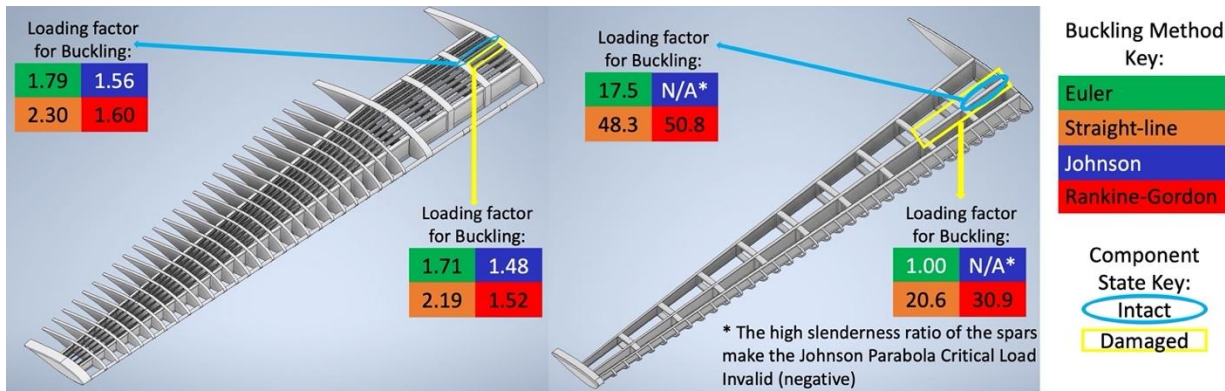


Figure 19. Buckling locations in the starboard wing (left) and horizontal stabilizer (right)

9.0 Conclusions from Analyses

Major Colton had a very successful career in the RCAF and now serves as an inspiration to women throughout aviation. Flying primarily in SAR applications she totaled over 6,900 hours of flight time in the CC-130E. The group used her flight style to guide analysis of the aircraft. Through the examination of multiple loading scenarios Group 03 determined that a clean, minimum radius 60 degree bank turn represented the worst case loading. With respect to this loading scenario, analyses of the starboard wing and horizontal stabilizer have been completed. First, a beam bending model of the wing was completed. Using the Rayleigh-Ritz method displacement and stress in the wing was found. The wing did not fail under normal conditions. In beam bending failure was induced 4.95 m from the fuselage with a variable load factor of 1.82. By removing the portion of the wing outboard of the failure location the damaged configuration was evaluated. In the damaged configuration the starboard wing failed under normal loading. The stabilizer was also analyzed using the beam bending model. For the horizontal stabilizer a load factor of 6.16 was required to cause failure at the root. No damaged configuration of the stabilizer beam bending model was analyzed.

Next, the group created a single-cell web stringer model of both the wing and horizontal stabilizer. This model more accurately reflected the locations and magnitudes of the stresses in each of the main spars and skins. Again, at the maximum rated centripetal acceleration no failure occurred. An increase of 11.4 m/s while maintaining the 583 m radius caused failure in the top flange of the leading spar. In the pre-damaged condition, an increase in airspeed of only 2.4 m/s from standard conditions was required to cause further failure. The stabilizer also did not fail until 227 m/s and 191 m/s in the intact and damaged condition, respectively.

The most accurate analysis performed is the multi-cell web-stringer analysis of the wing and horizontal stabilizer. The high accuracy comes in the fact that this is the most detailed representation of the structure of each component. This analysis is similar to the single-cell web-stringer analysis, except the wing and stabilizer are divided into multiple cells composed of all the structural elements. The multi-cell analysis includes more of the structural elements, and more accurately shows us the forces and stresses in each element. In multi-cell analysis, both wing and stabilizer underwent failure at the root. In the intact wing, failure occurred when variable loads were multiplied by a factor of 1.93, and the damaged wing failed under a factor of

1.64. The intact horizontal stabilizer failed when a load factor of 5.85 was applied, and the damaged condition failed under normal loading conditions.

Sheet buckling was analyzed in the web elements of the wings. The shear stresses calculated from the multi-cell web-stringer analysis was compared against the loads published by Boeing. Analysis indicated that skin buckling occurred in the wing along the leading edge panel inboard of the first engine. Skin buckling did not occur in the horizontal stabilizer under normal loading conditions.

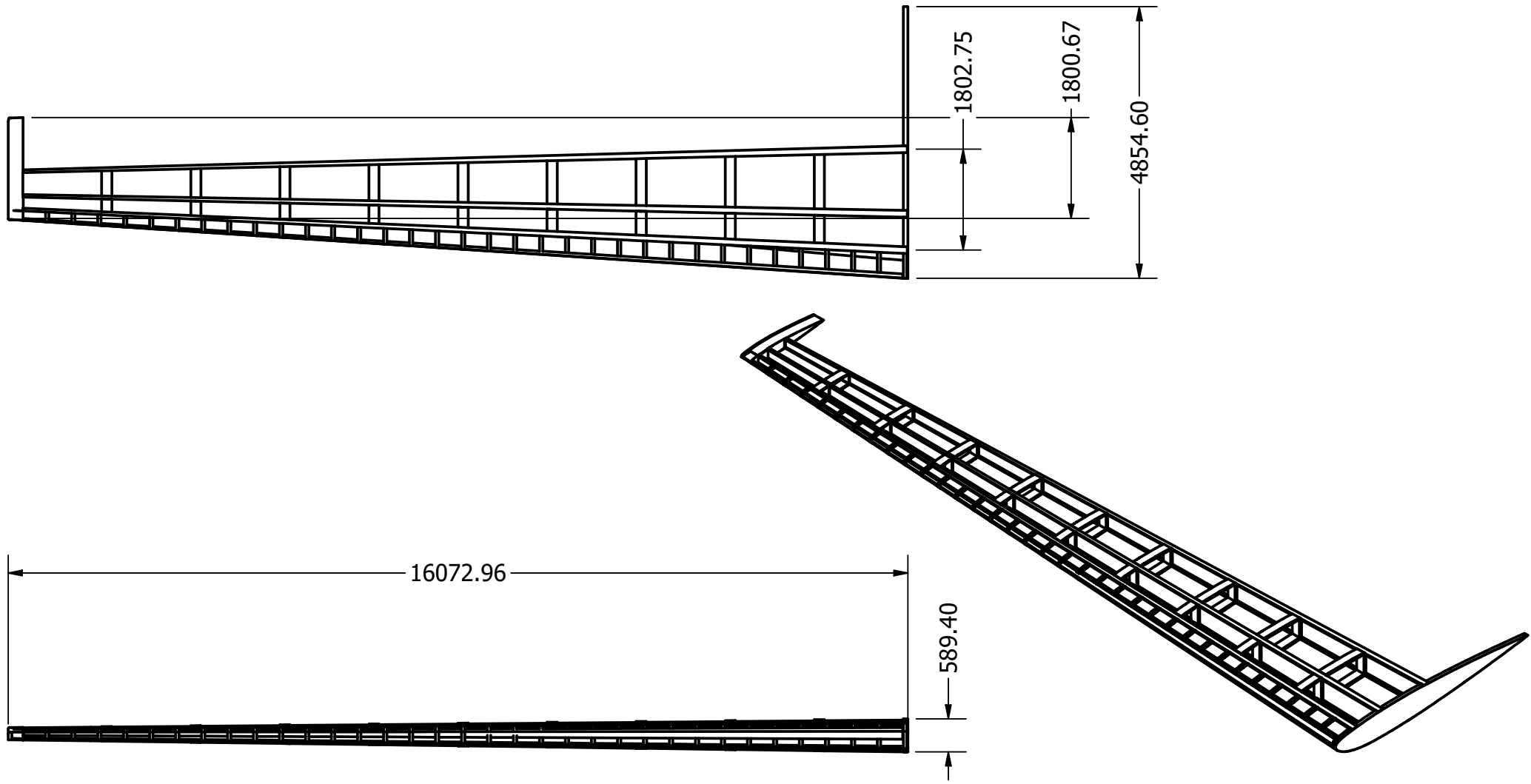
Additionally, the multi-cell web-stringer was analyzed under buckling failure criteria. Equations for four different buckling criteria were created, and the results compared to the forces in the spars. Under normal loading conditions, it was found that none of the spars or stringers in either the wing or stabilizer failed under buckling failure criteria. A loading factor of 1.48 was applied to the wing to induce the first failure in buckling in the wing using Johnson's method. In the horizontal stabilizer, a load factor of 17.5 was applied to induce the first failure using Euler's method. The horizontal stabilizer saw further failures under normal loading.

Group 03 would like to acknowledge and thank the National Air Force Museum of Canada for providing information on the CC-130E that has allowed for the completion of the analyses to date. Furthermore, the group would like to thank Major Michelle Colton for the opportunity to interview her and learn more about her career and the CC-130E she flew.

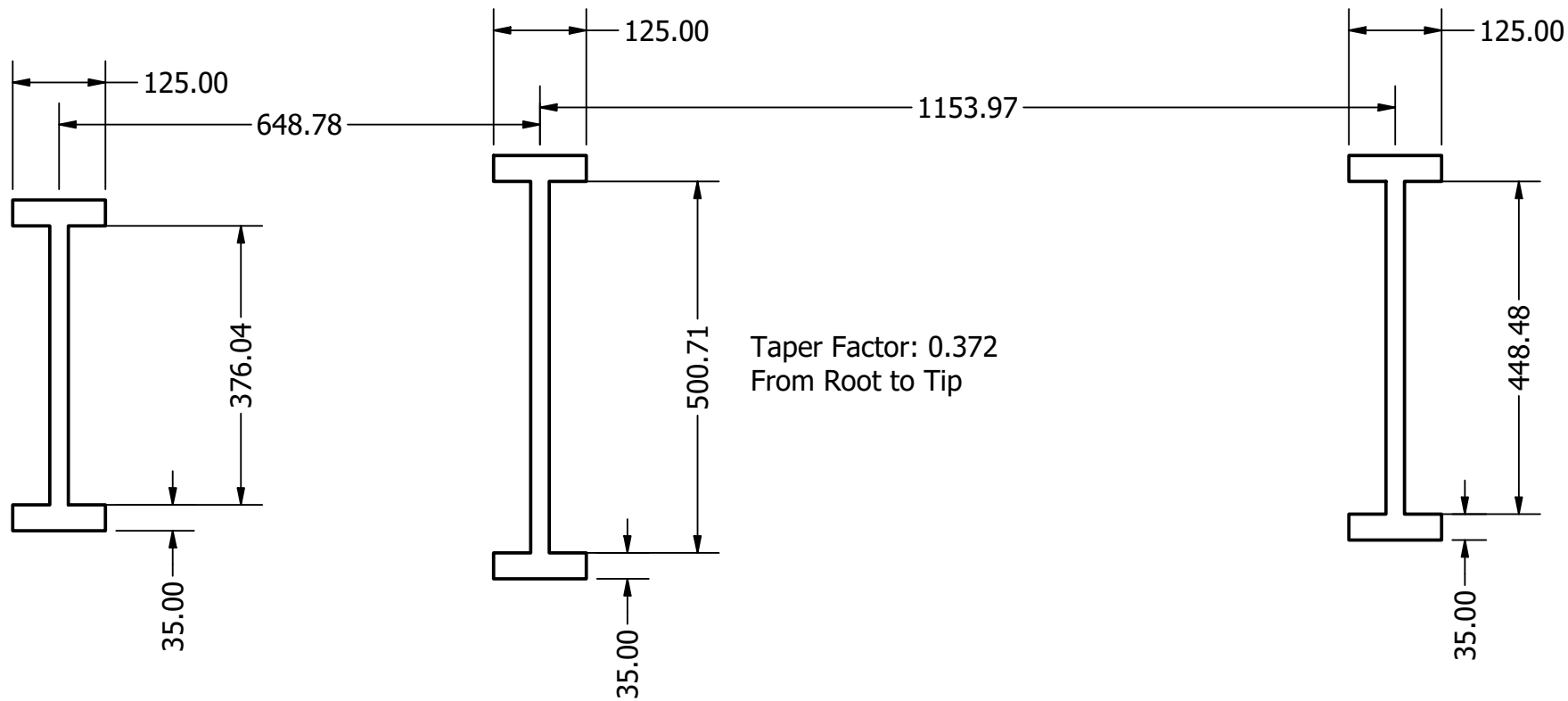
List of References

- [1] “Lockheed CC-130E Hercules military transport airplane,” Canada.ca, 05-Apr-2016. [Online]. Available: <https://www.canada.ca/en/department-national-defence/news/2016/04/lockheed-cc-130e-hercules-military-transport-airplane.html>. [Accessed: 04-Oct-2021].
- [2] T. Brooks, J. DiMeo, H. Garramone, M. Madonia, and M. Colton, “Major Michelle Colton: RCAF Career and Personal Life,” 15-Oct-2021.
- [3] J. Robinson, Ed., Elsie Pioneer Award, Maj. Micky Colton, vol. 60, no. 1, p. C6, Jan-2019.
- [4] Yoon, Hannah. “Couple Continues to Play Role in Military after Their Retirement.” The Pioneer, 13 Nov. 2013.
- [5] L. Bailey, “8 Wing Pilot Honored,” Royal Canadian Air Force. RCAF, 19-Aug-2009.
- [6] A. Francis, “From the air force, to horse farm owner to author, how a Mohawk woman is battling the pandemic,” APTN National News, 30-May-2021. [Online]. Available: <https://www.aptnnews.ca/national-news/micky-colton-mohawk-woman-horse-farm-author/>. [Accessed: 09-Oct-2021].
- [7] E. Mountney-Lessard, “End of an era,” The Kingston Whig Standard, 05-Apr-2016. [Online]. Available: <https://www.thewhig.com/2016/04/05/end-of-an-era/wcm/7240de05-6a91-c291-db28-09f0250c99de/amp/>. [Accessed: 09-Oct-2021].
- [8] “Hercules,” National Air Force Museum of Canada. [Online]. Available: http://airforcemuseum.ca/eng/?page_id=564. [Accessed: 11-Sep-2021].
- [9] “C-130 Hercules,” U.S. Air Force, 20-Jun-2018. [Online]. Available: <https://www.af.mil/About-Us/Fact-Sheets/Display/Article/1555054/c-130-hercules/>. [Accessed: 11-Sep-2021].
- [10] C. I. Gale, Ed., “Meet the Hercules ,” Service New , vol. 16, p. 6, 1989.
- [11] “USCG Lockheed C-130 Flight Manual.” United States Coast Guard, 15-Dec-2000,
- [12] J. Balle, “Rolls-royce T56 turboprop engine,” PowerWeb. [Online]. Available: <http://www.fi-powerweb.com/Engine/Rolls-Royce-T56.html>. [Accessed: 15-Sep-2021].
- [13] Lockheed Aircraft Corporation, “Aerodynamic Data for Structural Loads.” Burbank, CA, 02-Mar-1953.

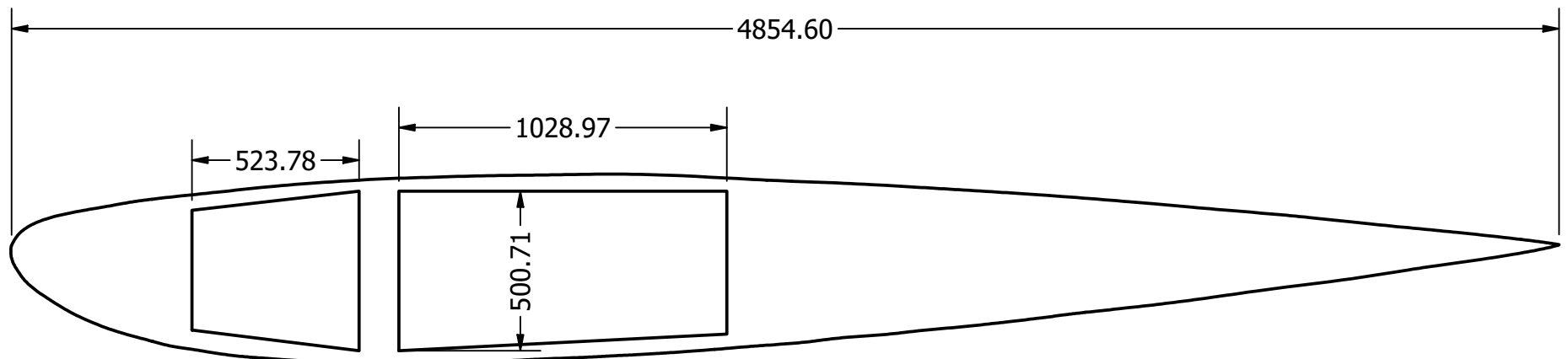
- [14] H. J. Singletary, "The Hercules Aircraft: A study in Evolving Materials and Processes Technology" vol 8, no.3, p.5, Sep-1981.
- [15] "Course Training Manual for CC130 Hercules Airframe Technician." 426 Training Squadron, Mar-1984, Trenton, Ontario.
- [16] Boeing Commercial Airplane Company, "Boeing Design Manual", n.d.
- [17] L. Imrie, private communication, Sep. 24, 2021
- [18] G. Maddux, "Stress Analysis Manual", Technology Incorporated, Dayton, Ohio, 1969



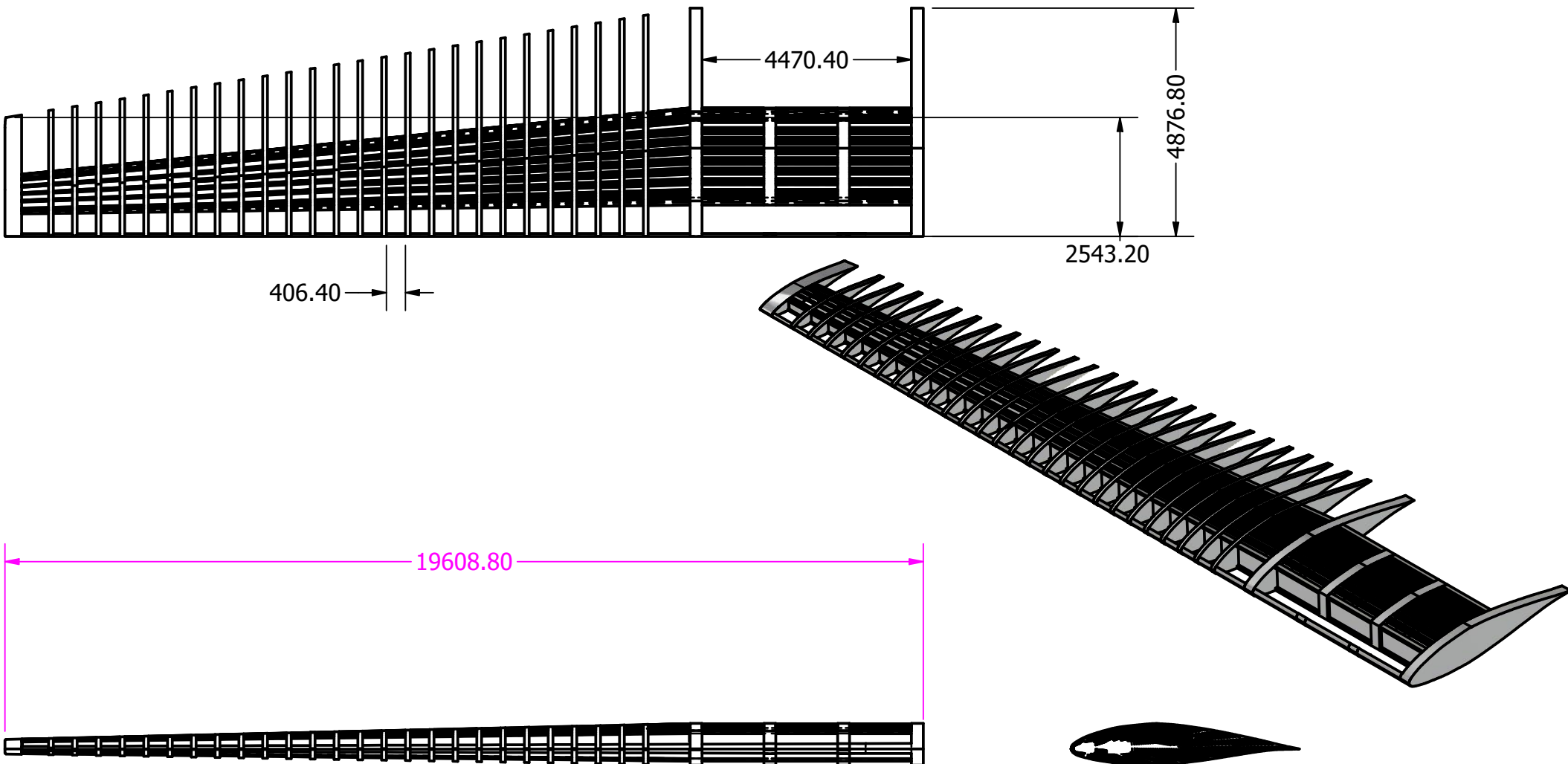
DRAWN micha	10/29/2021	Group 03		
CHECKED				
QA		TITLE		
MFG		Starboard Horizontal Stabilizer Assembly		
APPROVED				
	SIZE A	DWG NO StarboardStabfinal	REV	
	SCALE 1 / 100		SHEET 1 OF 3	



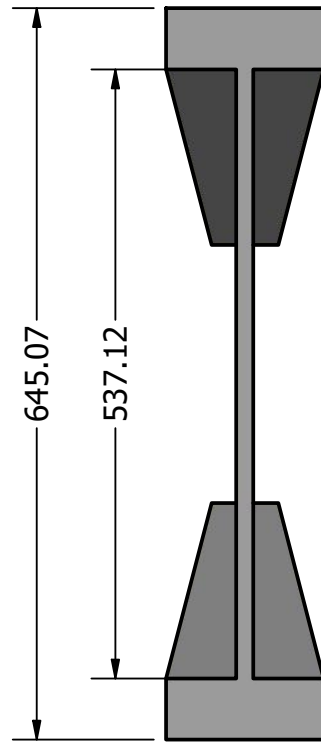
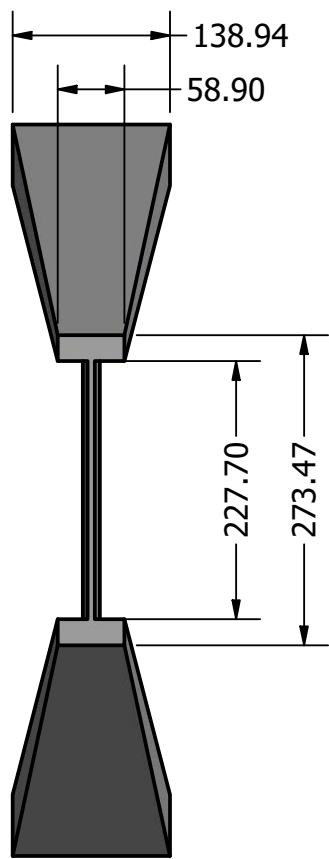
DRAWN micha	CHECKED	10/29/2021	Group 03		
QA			TITLE		
MFG			Spar Cross Section and Layout at Root of Horizontal Stabilizer		
APPROVED			SIZE A	DWG NO StarboardStabfinal	REV
			SCALE 0.11		SHEET 2 OF 3



DRAWN micha	10/29/2021	Group 03		
CHECKED				
QA		TITLE		
MFG		Rib at Root of Horizontal Stabilizer		
APPROVED		SIZE A	DWG NO StarboardStabfinal	REV
		SCALE 0.05		SHEET 3 OF 3

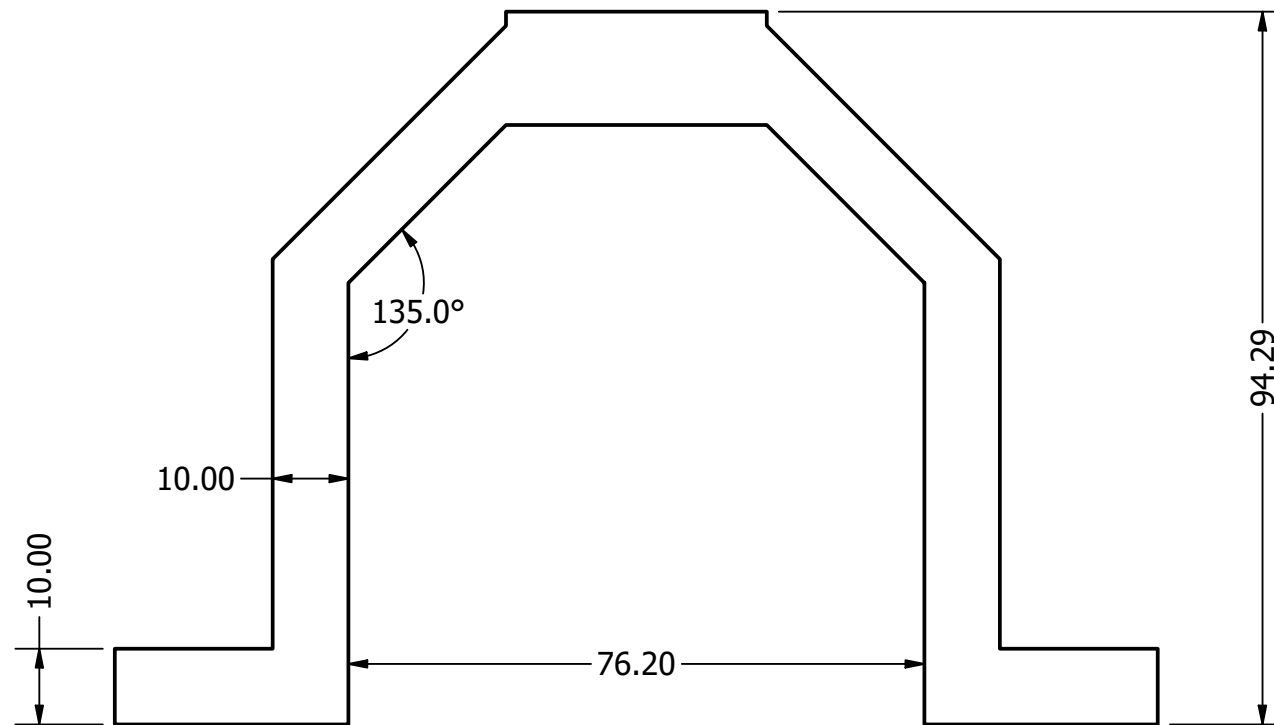


DRAWN	Michael Madonia	10/21/2021	Group 03		
CHECKED					
QA			TITLE		
MFG			Starboard Wing Assembly		
APPROVED			SIZE	DWG NO	REV
			A	starboardWingfinal	
			SCALE	1 / 120	SHEET 4 OF 5

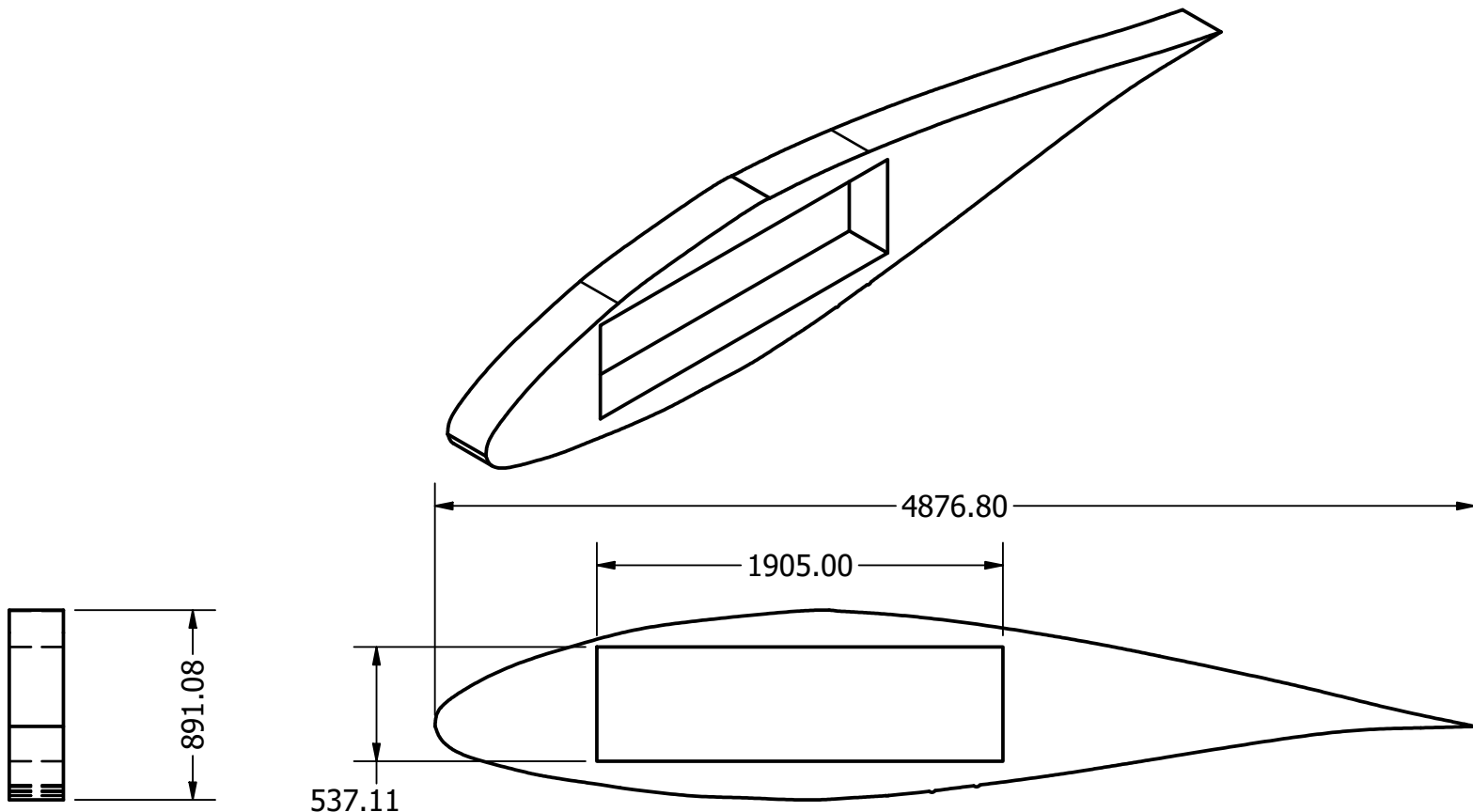


Taper Factor: 0.522

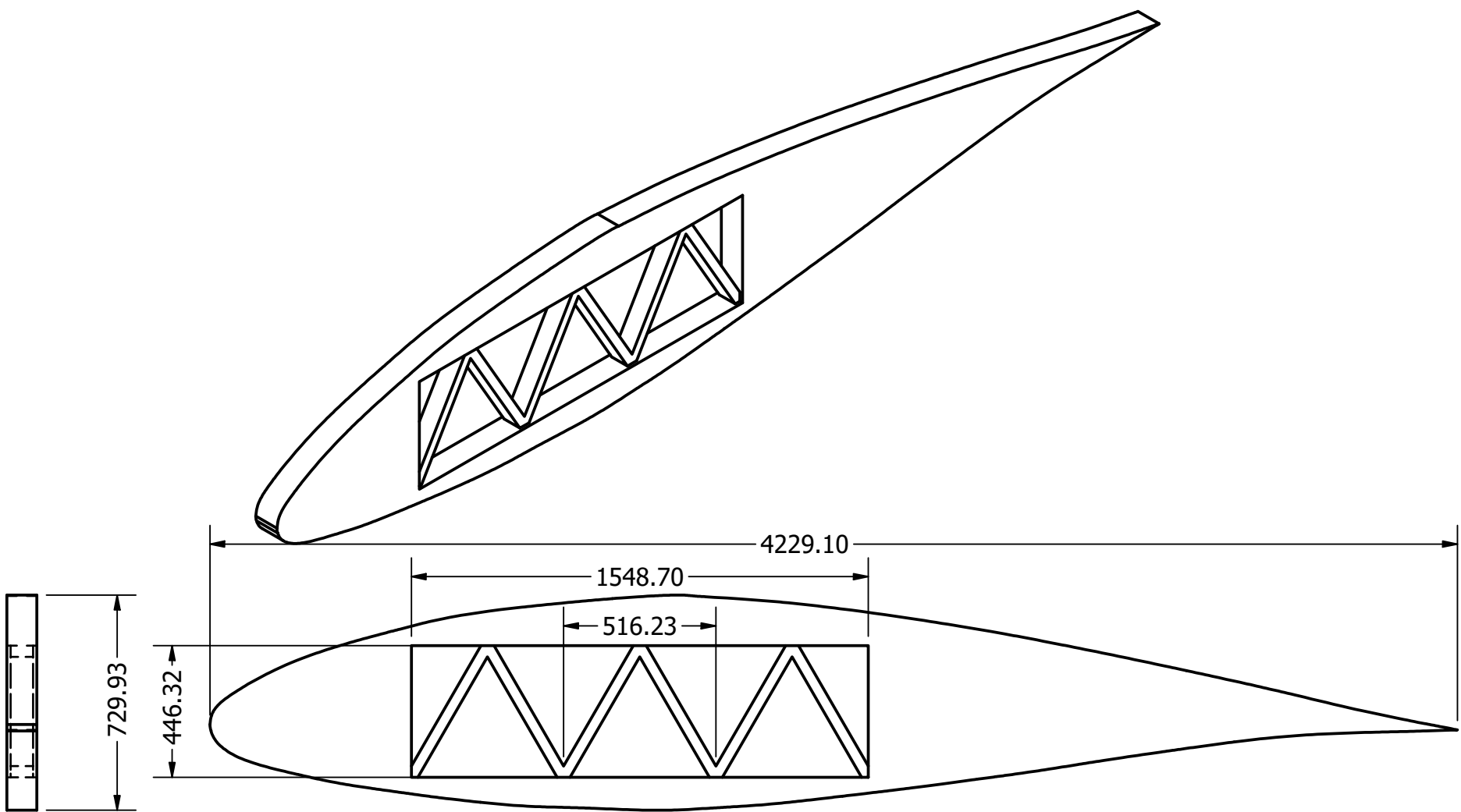
DRAWN	Michael Madonia	10/21/2021	Group 03		
CHECKED			TITLE		
QA			Spar		
MFG			Taper Factor: 0.522		
APPROVED			SIZE		DWG NO
			A		starboardWingfinal
			SCALE	.15	REV
					SHEET 1 OF 5



DRAWN	Michael Madonia	10/21/2021	Group 03
CHECKED			
QA			TITLE
MFG			Stringer Cross Section at Root Taper Factor: 0.522
APPROVED			SIZE DWG NO
		A	starboardWingfinal
		SCALE 1 : 1	REV
			SHEET 5 OF 5



DRAWN Michael Madonia	10/21/2021	Group 03		
CHECKED				
QA		TITLE		
MFG		Rib at Root		
APPROVED		SIZE A	DWG NO starboardWingfinal	REV
		SCALE 0.03		SHEET 2 OF 5



DRAWN	Michael Madonia	10/21/2021	Group 03
CHECKED			
QA			TITLE
MFG			Rib with Truss Structure
APPROVED			
	SIZE A	DWG NO starboardWingfinal	REV
	SCALE 0.05		SHEET 3 OF 5